© 2017. Published by The Company of Biologists Ltd | Journal of Cell Science (2017) 130, 396-405 doi:10.1242/jcs.192450

RESEARCH ARTICLE

# Super-resolution microscopy reveals the insulin-resistance-regulated reorganization of GLUT4 on plasma membranes

**Lan Gao[1,2], Junling Chen[2,3], Jing Gao[2,3], Hongda Wang[3,*] and Wenyong Xiong[1,*]**

## ABSTRACT

GLUT4 (also known as SLC2A4) is essential for glucose uptake in skeletal muscles and adipocytes, which play central roles in whole-body glucose metabolism. Here, using direct stochastic optical reconstruction microscopy (dSTORM) to investigate the characteristics of plasma-membrane-fused GLUT4 at the single-molecule level, we have demonstrated that insulin and insulin resistance regulate the spatial organization of GLUT4 in adipocytes. Stimulation with insulin shifted the balance of GLUT4 on the plasma membrane toward a more dispersed configuration. In contrast, insulin resistance induced a more clustered distribution of GLUT4 and increased the mean number of molecules per cluster. Furthermore, our data demonstrate that the $F^5QQI$ motif and lipid rafts mediate the maintenance of GLUT4 clusters on the plasma membrane. Mutation of $F^5QQI$ ($F^5QQA$-GLUT4) induced a more clustered distribution of GLUT4; moreover, destruction of lipid rafts in adipocytes expressing $F^5QQA$-GLUT4 dramatically decreased the percentage of large clusters and the mean number of molecules per cluster. In conclusion, our data clarify the effects of insulin stimulation or insulin resistance on GLUT4 reorganization on the plasma membrane and reveal new pathogenic mechanisms of insulin resistance.

**KEY WORDS: GLUT4, Insulin resistance, Direct stochastic optical reconstruction microscopy, dSTORM, Membrane protein**

## INTRODUCTION

Membrane proteins controlling molecular transport are required to maintain cell function. Glucose transporters essentially gate hexose transport through the plasma membrane to mediate energy metabolism. In particular, glucose transporter 4 (GLUT4; also known as SLC2A4) is specifically expressed in insulin-responsive adipose tissue and skeletal muscles, and functions to control cellular glucose metabolism and whole-body energy homeostasis.

GLUT4 is a key player in both normal glucose homeostasis and insulin resistance, which is strongly linked to type 2 diabetes and is associated with reduced uptake of glucose by muscles and adipose tissues. GLUT4 is responsible for this uptake, and the function of GLUT4 is disrupted in the insulin-resistant state.

The mechanisms of GLUT4 sorting have been extensively studied. In the absence of insulin, only 5% of the total GLUT4 is present in the plasma membrane, where it catalyzes the facilitated diffusion of glucose into the cells; in contrast, the majority of GLUT4 is maintained in intercellular compartments, such as endosomes, the trans-Golgi network and GLUT4-specialized vesicles (GSVs) (Martin et al., 2000; Slot et al., 1991). Increased serum glucose levels following a meal or rapid exercise induce release of insulin from the pancreas, resulting in redistribution of half of the cell's GLUT4 contents to the plasma membrane; this promotes glucose uptake, metabolism and energy storage in the adipose tissues and/or skeletal muscles. Failure of GLUT4 translocation to the plasma membrane in response to insulin is a predominant clinical symptom of insulin resistance and type 2 diabetes mellitus (Watson et al., 2001). Moreover, the plasma membrane is the main site for GLUT4 function and recycling, and plasma-membrane-fused GLUT4 exists in clusters or monomers (Bai et al., 2007; Gonzalez and McGraw, 2006; Gustavsson et al., 1996; Huang et al., 2007; Jiang et al., 2008; Koumanov et al., 2005; Lizunov et al., 2005; Parton et al., 2002; Stenkula et al., 2010). However, the characteristics of GLUT4 organization on the plasma membrane, particularly in the context of disease states, have not been examined at the single-molecule level owing to limitations in traditional microscopy.

In this study, we applied direct stochastic optical reconstruction microscopy (dSTORM) (Heilemann et al., 2008) to systematically investigate the patterns of GLUT4 fusion with plasma membrane in the basal and insulin-stimulated states in resting and insulin-resistant adipocytes at high resolution (tens of nanometers) in adipocytes. Our data provide important insights into GLUT4 organization on the plasma membrane.

## RESULTS

### Insulin regulates GLUT4 clustering on the plasma membrane

To visualize plasma-membrane-fused GLUT4, we stably expressed an exogenous GLUT4 vector in differentiated 3T3-L1 adipocytes. This vector, designated HA–GLUT4–GFP comprises a hemagglutinin (HA) epitope in the first exofacial loop of human GLUT4 and green florescent protein (GFP) fused to the carboxyl domain (Fig. S1A) (Lampson et al., 2000). The cells were immunostained with an Alexa-Fluor 647-conjugated antibody against HA.11 under nonpermeabilized conditions at a saturated concentration to ensure complete labelling of cell surface HA–GLUT4–GFP (Fig. S1B–F).

dSTORM was used to image and analyze the spatial patterning of GLUT4 at the surface of HA–GLUT4–GFP-expressing adipocytes under basal and insulin-stimulated (100 nM for 8 min) conditions, and in cells after removal of insulin (Fig. 1A). This approach permitted us to directly observe GLUT4 distribution on the plasma membrane at a resolution of nearly 30 nm (Fig. S2). Single GLUT4 molecules and clusters were clearly visible at the single-molecule level (Fig. 1B). The density of GLUT4 molecules and clusters at the cell surface was increased in insulin-stimulated adipocytes

[1]State Key Laboratory of Phytochemistry and Plant Resources in West China, Kunming Institute of Botany, Chinese Academy of Sciences, Kunming, Yunnan 650201, P.R. China. [2]Graduate University of Chinese Academy of Sciences, Beijing 100049, P.R. China. [3]State Key Laboratory of Electroanalytical Chemistry, Changchun Institute of Applied Chemistry, Chinese Academy of Sciences, Changchun, Jilil 130022, P.R. China.

*Authors for correspondence (xiong.wenyong@mail.kib.ac.cn; hdwang@ciac.ac.cn)

W.X., 0000-0001-9174-3667

**Received 18 May 2016; Accepted 11 November 2016**

Journal of Cell Science (2017) 130, 396-405 doi:10.1242/jcs.192450

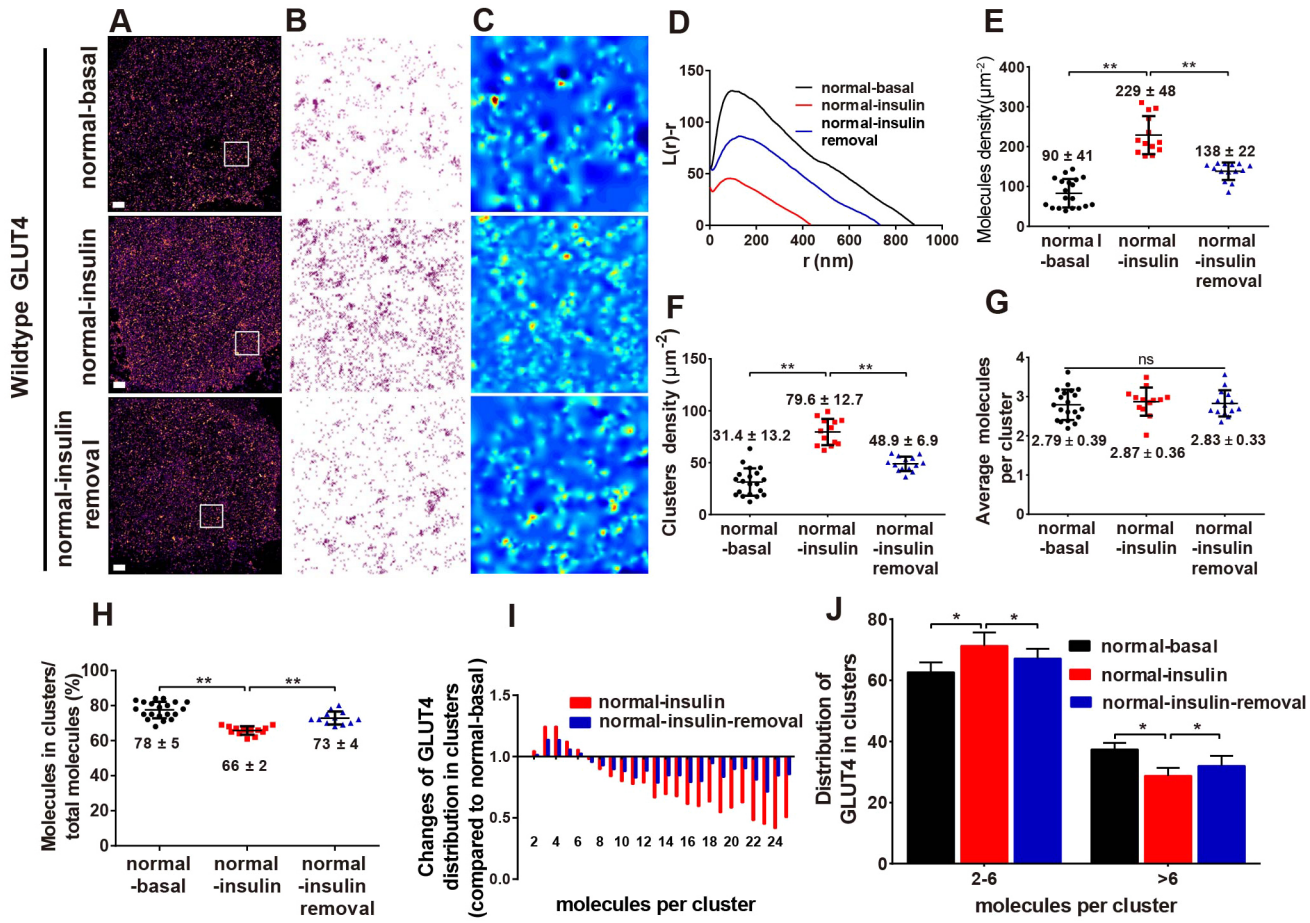


**Fig. 1. Insulin promotes GLUT4 organization on the plasma membrane in normal adipocytes.** (A) Representative dSTORM images of GLUT4 distribution on the plasma membrane of adipocytes that stably expressed HA–GLUT4–GFP in basal (normal-basal) and insulin-stimulated (normal-insulin) conditions, and after insulin removal (normal-insulin removal) conditions. The cells were fixed and stained with Alexa-Fluor-647-conjugated anti-HA antibodies under nonpermeabilized conditions with excitation with a 640-nm laser. Scale bars: 2 µm. (B) Enlarged and background-adjusted images illustrate the GLUT4 distribution patterns on the plasma membrane in the white-boxed regions (4×4 µm) shown in A. (C) Heat maps of GLUT4 clustering corresponding with the regions outlined in A, generated from a local point-pattern analysis. The colors indicate the degree of clustering from low (blue) to high (red). (D) Representative plot of Ripley's *K* function analysis of the clustering abilities of GLUT4 molecules in the white-boxed regions of A. *L*(*r*)-*r* (*y*-axis) represents the clustering ability, and *r* (*x*-axis) represents the radial scales of clustering. (E–H) Characteristics of GLUT4 distribution on the plasma membrane under the indicated conditions. The molecule density (E), cluster density (F), mean molecules per cluster (G) and percentage of clustered GLUT4 molecules relative to the total number of GLUT4 molecules (H) were obtained from dSTORM images (A) and calculated by using GDSC SMLM software (mean±s.d.). ns, not significant; **P*<0.01, ***P*<0.0001, two-tailed paired Student's *t*-tests. (I) Changes in the portion of GLUT4 molecules inside the clusters under insulin-stimulated conditions or after insulin removal as compared with the values of similarly sized clusters under basal conditions. (J) Quantification of the percentage of GLUT4 molecules in clusters having sizes between two and six molecules or more than six molecules relative to the total number of GLUT4 molecules, summarized from data shown in I. Data were from 20 cells (basal), 13 cells (insulin) and 14 cells (insulin-removal) from three independent experiments. In E–H, every point represents one single cell. **P*<0.01, ***P*<0.0001; ns, not significant; two-tailed paired Student's *t*-test. Data are mean±s.d.

compared with that on adipocytes under basal conditions. We then used quantitative cluster analysis based on Ripley's *K* function (Owen et al., 2010) to calculate the cluster maps (Fig. 1C). There were more GLUT4 clusters after insulin stimulation, although the degree of clustering was lower than that in the basal state. After removal of insulin for 30 min, the distribution of plasma membrane GLUT4 recovered to a basal-condition-like pattern.

To quantitatively analyze the differences in plasma membrane GLUT4 distribution between these states, we used Ripley's *K* function to measure the spatial clustering of nanoscale domains of GLUT4. The averaged Ripley's *L(r)-r* plots for the representative regions from cells under different conditions are shown in Fig. 1D. Analysis of 10–20 different cells (nine regions per individual cell) yielded nearly identical results – Ripley's *K*-function plots peaked at higher clustering values for GLUT4 at the surface of basal adipocytes than in insulin-stimulated adipocytes, suggesting that GLUT4 on the plasma membrane was less clustered because of insulin. GLUT4 in cells under basal conditions remained clustered at scales of over 800 nm, whereas for insulin-stimulated cells, the protein became less clustered or exhibited a random distribution beyond 400 nm. After removal of insulin, the density of clusters and the largest radius of the cluster were similar to those found under basal conditions.

Additionally, quantitative analyses of dSTORM data by using GDSC SMLM software allowed for evaluation of several parameters in order to describe the differences in the clusters in different states and to confirm the results of Ripley's *K* function analysis. The number of molecules/µm$^2$ and clusters/µm$^2$ of plasma membrane GLUT4 increased by nearly 2.5-fold with insulin stimulation, from 90±41 molecules/µm$^2$ (mean±s.d.) and 31.4±13.2 clusters/µm$^2$ in cells under basal conditions to 229±48 molecules/µm$^2$ and 79.6±12.7 clusters/µm$^2$ after stimulation. After

Journal of Cell Science (2017) 130, 396-405 doi:10.1242/jcs.192450

insulin removal, there were 138±22 molecules/μm$^2$ and 48.9±6.9 clusters/μm$^2$ on the plasma membrane (Fig. 1E,F). The mean number of molecules per cluster did not significantly change after insulin stimulation, with 2.79±0.39/μm$^2$ in basal conditions, 2.87±0.36/μm$^2$ under insulin-stimulated conditions, and 2.83±0.33/μm$^2$ after removal of insulin (Fig. 1G). Interestingly, we found a lower fraction of GLUT4 in clusters on the plasma membrane of insulin-stimulated cells (66±2%; mean±s.d.) than in cells under basal conditions (78±5%), indicating that fewer molecules formed GLUT4 clusters in insulin-stimulated adipocytes (Fig. 1H). The proportion of proteins in differently sized clusters (which contained different numbers of proteins) was then determined (Fig. 1I; Fig. S3A). Notably, the proportion of GLUT4 molecules in small clusters (the mean number of proteins per cluster ranged from 2 to 6) markedly increased, and the proportion of molecules that were found in large clusters (the average number of proteins per cluster was greater than 6) decreased as the number of proteins per cluster increased. Indeed, 10% of proteins in large clusters were shifted to form small clusters (with an average number of proteins per cluster of 2–6) (Fig. 1J). In summary, the decrease in clustered GLUT4 and the shift of the molecules from large clusters to small clusters made the distribution of plasma membrane GLUT4 more disperse in response to insulin. Insulin removal after insulin stimulation partially recovered the insulin-induced changes in cluster characteristics.

### Insulin resistance reorganizes the clustering of plasma membrane GLUT4

Previous studies have shown that several steps in GLUT4 translocation are regulated by insulin resistance. However, whether the clustering of GLUT4 on the plasma membrane is altered in insulin-resistant adipocytes remains unknown. To address this question, GLUT4 on the surface of adipocytes in the insulin-resistant state were imaged and analyzed. Insulin resistance was successfully established by overnight incubation with 100 nM insulin, as verified by western blotting (Fig. S4) (Xiong et al., 2010). The phosphorylation of Akt at residues Thr308 and Ser473 (detected using antibodies against phosphorylated Akt that recognize phosphorylation of Akt1, Akt2 and Akt3 at corresponding residues) and of AS160 at residue Thr642 was inhibited in response to insulin stimulation owing to insulin resistance, consistent with a previous report (Fazakerley et al., 2015).

Next, super-high resolution images of GLUT4 patterning on the surface of insulin-resistant adipocytes under basal or insulin-stimulated conditions (IR-basal and IR-insulin, respectively) were obtained, and the cluster features were analyzed (Fig. 2A–C). A more-clustered distribution was observed under both conditions compared with that in normal cells.

Analysis using Ripley's *K* function (Fig. 2D) showed that insulin stimulation moderately reduced GLUT4 cluster formation. The extent of the reduction of the peak value induced by insulin in insulin-resistant cells (about 36%, from 250 to 160) was not as large as that in normal cells (about 70%, from 130 to 40; Figs 1D and 2D). In addition, by comparing the maximum *L(r)-r* value, whether cells were in the basal or insulin-stimulated state, GLUT4 was more clustered on the surface of insulin-resistant cells than on the surface of normal cells. The mean diameters of GLUT4 clusters were similar under basal and insulin-stimulated conditions, whereas the theoretically predicted maximum scale ($r_{max}$) of clusters was slightly reduced from 700 to 600 nm in response to insulin (Fig. 2D).

Statistical analysis of GLUT4 cluster properties showed that the number of molecules/μm$^2$ and clusters/μm$^2$ of plasma membrane GLUT4 increased slightly with insulin stimulation in insulin-resistant adipocytes, from 116±26 molecules/μm$^2$ and 35.4±6.2 clusters/μm$^2$ in cells under basal conditions to 154±52 molecules/μm$^2$ and 45.9±16.9 clusters/μm$^2$ in insulin-stimulated cells (Fig. 2E,F). These data indicate that insulin resistance reduced the sensitivity of cells to insulin in half in our system, consistent with the western blotting data. Furthermore, insulin did not significantly alter the mean number of molecules per cluster (3.27±0.37 in basal conditions, 3.41±0.39 in insulin-stimulated conditions; $P$=0.257) or the distribution of molecules in differently sized clusters (Fig. 2G,I); however, there was a small reduction in the fraction of the total number of molecules that was found in clusters (Fig. 2H). These features did not dramatically change after ablation of insulin sensitivity in insulin-resistant cells. However, in both the basal and insulin-stimulated states, the mean number of GLUT4 molecules per cluster was increased by approximately 20%, and the fraction of molecules in clusters increased by nearly 10% (84±2% of IR-basal cells and 78±4% of IR-insulin cells; Fig. 2G,H). The proportion of total molecules found in large clusters on the surface of IR-basal or IR-insulin cells was also increased compared with that on normal cells under basal conditions (Fig. 2J; Fig. S3B). This further confirmed that plasma membrane GLUT4 became more clustered in the insulin-resistant state.

### Mutation of F$^5$QQI induces a more clustered distribution of GLUT4 on the plasma membrane

Previous studies have suggested that plasma membrane GLUT4 clusters colocalize with clathrin-coated pits in adipocytes through involvement of the adaptor protein AP2, which recognizes and interacts with the N-terminal F$^5$QQI motif of GLUT4 (Al-Hasani et al., 2002; Owen et al., 2004; Stenkula et al., 2010). Therefore, we hypothesized that the F$^5$QQI motif might be associated with the maintenance of plasma membrane GLUT4 clusters.

We mutated the F$^5$QQI motif of GLUT4 (F$^5$QQA-GLUT4) and expressed this construct in adipocytes; these adipocytes were used to block the association between plasma membrane GLUT4 clusters and clathrin-coated pits. dSTORM data showed that the plasma membrane F$^5$QQA-GLUT4 in basal and insulin-stimulated adipocytes still exhibited a clustered or dispersed distribution. Notably, the number of large clusters of F$^5$QQA-GLUT4 on the membranes of basal and insulin-stimulated cells was increased compared with that of wild-type GLUT4 clusters (Fig. 1A–C; Fig. 3A–C). Analysis using Ripley's *K* function revealed that the degree of F$^5$QQA-GLUT4 clustering was reduced by insulin stimulation (from 170 to 70; Fig. 3D). However, compared with wild-type GLUT4, F$^5$QQA-GLUT4 was more clustered on the surface of both cells under basal conditions and upon stimulation with insulin, whereas the clustering range and cluster diameter of plasma-membrane-fused F$^5$QQA-GLUT4 did not change markedly (Figs 1D and 3D).

Further analysis showed that insulin stimulation increased the number of F$^5$QQA-GLUT4 molecules and clusters on the plasma membrane (184±37 molecules/μm$^2$ and 49.8±11.0 clusters/μm$^2$ for adipocytes under basal conditions versus 363±123 molecules/μm$^2$ and 108.9±33.4 clusters/μm$^2$ for insulin-stimulated adipocytes; mean±s.d.; Fig. 3E,F). The mutation of GLUT4 induced an obvious increase in the mean number of molecules per cluster (3.73±0.36 in basal conditions and 3.44±0.33 in insulin-stimulated conditions), compared with that of wild-type GLUT4 (Fig. 3G; Table S1). Although the fraction of the total molecules found in clusters was not significantly altered in the presence of the mutation (80±4% in basal conditions versus 63±5% in insulin-stimulated conditions; Fig. 3H; Table S1), the distribution of F$^5$QQA-GLUT4 in differently sized clusters indicated that mutation of GLUT4

Journal of Cell Science (2017) 130, 396-405 doi:10.1242/jcs.192450

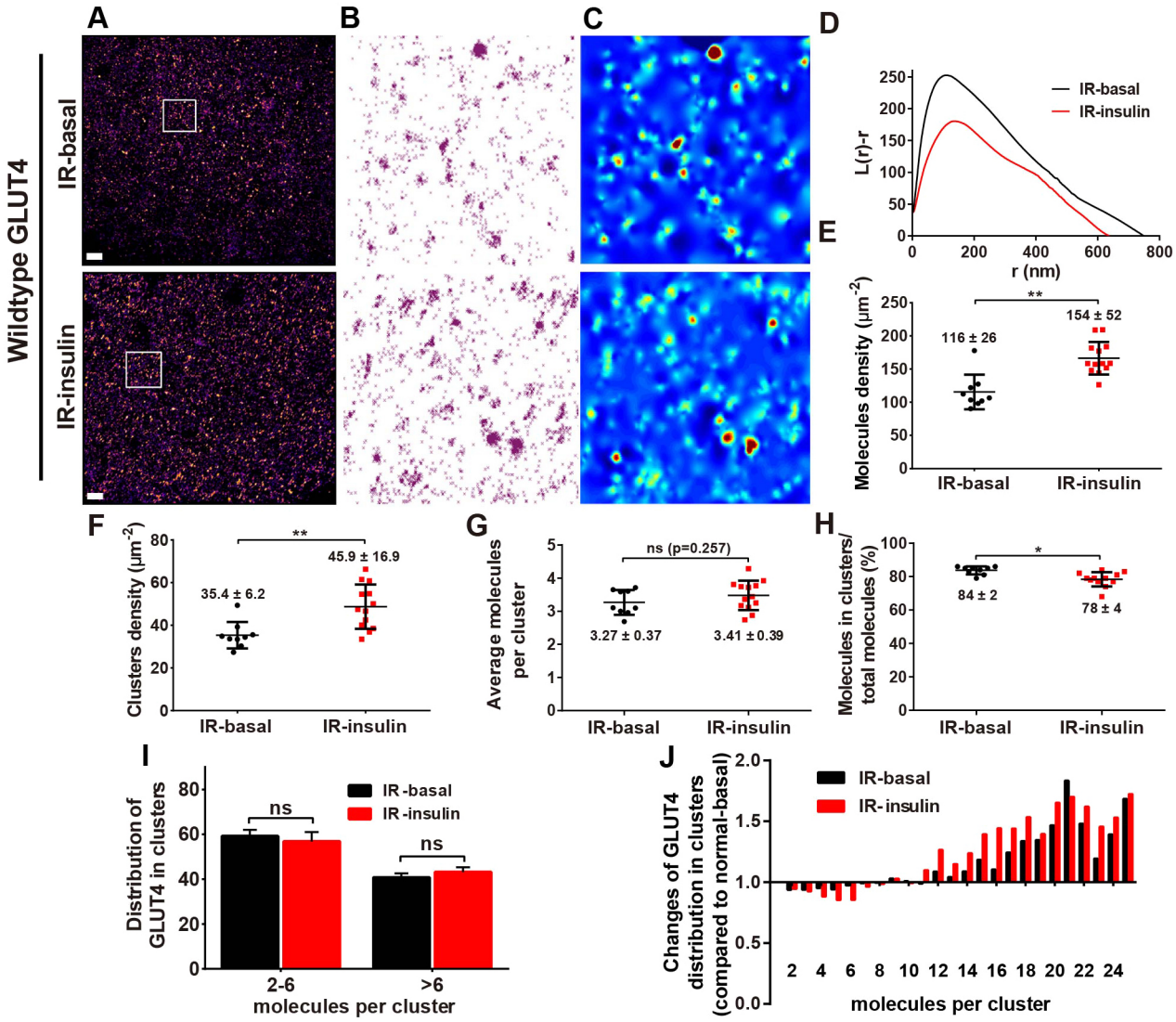


**Fig. 2. GLUT4 organization is regulated in insulin-resistant adipocytes.** (A) Representative dSTORM images of GLUT4 distribution on the plasma membrane of insulin-resistant adipocytes that stably expressed HA–GLUT4–GFP in basal (IR-basal) and insulin-stimulated (IR-insulin) states. Scale bars: 2 μm. The adipocytes were incubated with 100 nM insulin overnight and starved for 2 h before insulin stimulation. (B) Enlarged and background-adjusted images illustrated the GLUT4 distribution patterns on the plasma membrane in the white-boxed regions (4×4 μm) shown in A. (C) Heat maps of GLUT4 clustering from the white-boxed regions shown in A. (D) Representative plot of Ripley's *K* function analysis of the clustering abilities of GLUT4 molecules in the white-boxed regions of A. (E–H) Characteristics of GLUT4 distribution on the plasma membrane under the indicated conditions. Protein density (E), cluster density (F), mean molecules per cluster (G) and the percentage of clustered GLUT4 molecules relative to the total number of GLUT4 molecules (H) were obtained from dSTORM images (A) and calculated by using GDSC SMLM software (mean±s.d.). (I) Percentages of GLUT4 in clusters having sizes between two and six molecules, and more than six molecules. (J) Changes in GLUT4 molecules inside the clusters, as compared with GLUT4 under basal conditions in normal adipocytes. Data were from nine cells (IR-basal) or 12 cells (IR-insulin) from three independent experiments. In E–H, every point represents one single cell. ns, not significant; **P*<0.01, ***P*<0.0001; two-tailed paired Student's *t*-test. Data are mean±s.d.

reduced the population of $F^5$QQA-GLUT4 in small clusters and caused more mutants to form large clusters (Fig. 3I,J; Fig. S3C). These data show that mutation of GLUT4 promoted a more clustered distribution of GLUT4 on the plasma membrane both under basal and insulin-stimulated conditions.

### Destruction of lipid rafts disperses the distribution of $F^5$QQA-GLUT4 on the plasma membrane

Lipid rafts are platforms that function in signal transduction, molecular trafficking and protein assembly (Brown and London, 2003; Gao et al., 2015; Lingwood and Simons, 2010; Owen et al., 2012a; Pontier et al., 2008). To examine whether maintenance of GLUT4 clusters was associated with lipid rafts, 3T3-L1 adipocytes that stably expressed $F^5$QQA-GLUT4 were used and treated with methyl-β-cyclodextrin (MβCD) (to disrupt lipid rafts) only in the basal state. Fig. 4A–C shows changes in the distribution of $F^5$QQA-GLUT4 on the surface of basal adipocytes after incubation with 10 mM MβCD. We found that destruction of lipid rafts increased the densities of molecules and clusters on the membrane, and that most protein clusters became smaller or were even lost. The degree of $F^5$QQA-GLUT4 clustering under basal conditions was reduced to a level similar to that of wild-type GLUT4 (maximum *L(r)-r* of about 40; Fig. 4D). Cluster analysis of plasma membrane $F^5$QQA-GLUT4 indicated that there were 260±43 molecules/μm$^2$ (mean±s.d.) and 97.1±12.3 clusters/μm$^2$ on the plasma membrane after treatment with MβCD in the basal state (Fig. 4E). In addition, the mean number of

Journal of Cell Science (2017) 130, 396-405 doi:10.1242/jcs.192450

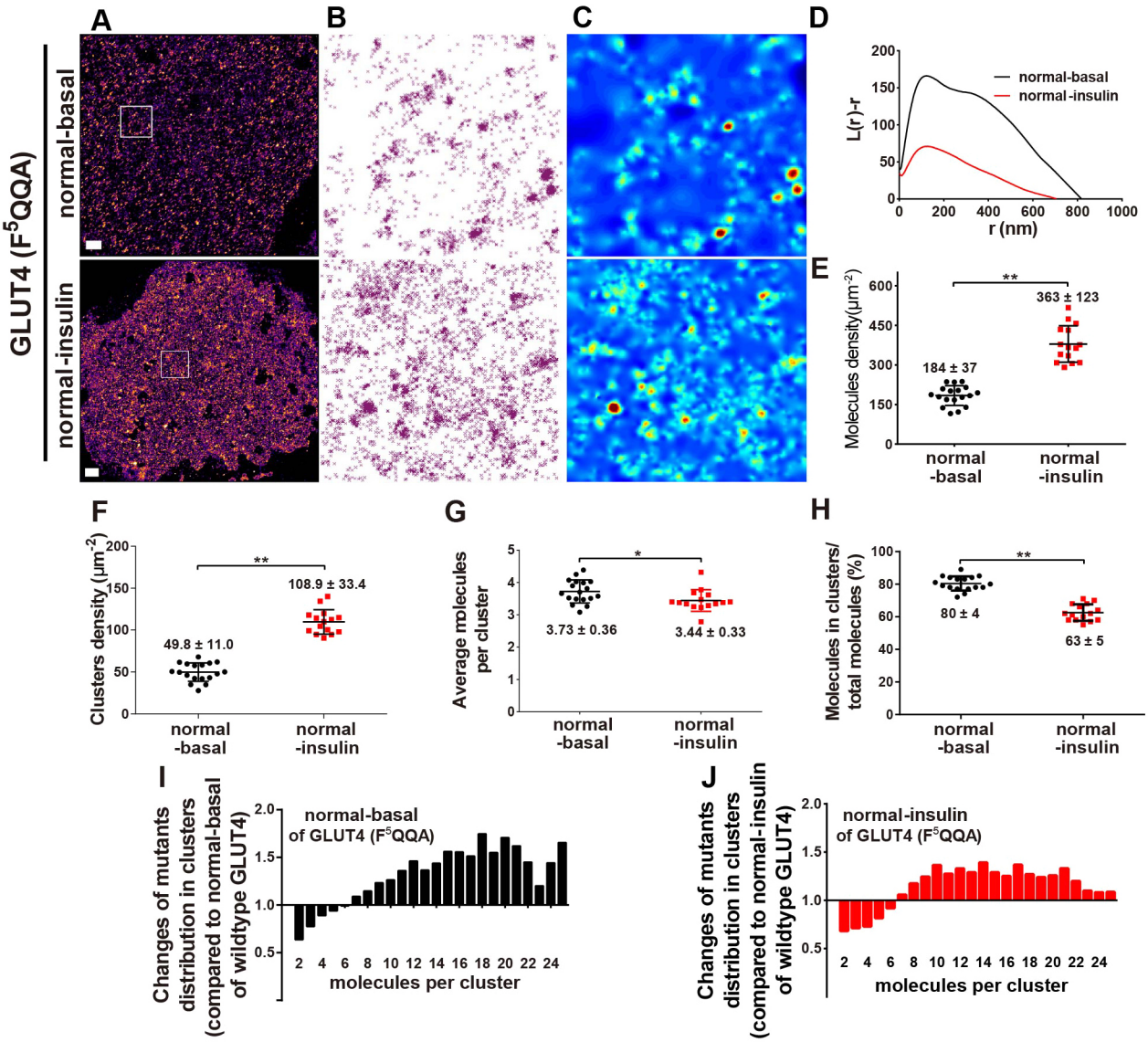


**Fig. 3. The F$^5$QQI motif is involved in GLUT4 organization on the plasma membrane of normal adipocytes.** (A) Representative dSTORM images of GLUT4 distribution on the plasma membrane of adipocytes that stably expressed HA– F$^5$QQA-GLUT4–GFP in basal and insulin-stimulated conditions. Scale bars: 2 µm. (B) Enlarged and background-adjusted images illustrated the GLUT4 distribution patterns on the plasma membrane of the white-boxed regions (4×4 µm) shown in A. (C) Heat maps of GLUT4 clustering from the white-boxed regions in A. (D) Ripley's *K* function analysis of the molecules in white-boxed regions in A. (E–H) Characteristics of the GLUT4 distribution on the plasma membrane under the indicated conditions. Protein density (E), cluster density (F), mean molecules per cluster (G) and percentage of clustered GLUT4 relative to the total number of GLUT4 molecules (H) were obtained from the dSTORM images shown in A and calculated using GDSC SMLM software (mean±s.d.). (I,J) Changes in F$^5$QQA-GLUT4 molecules in clusters under basal (I) or insulin-stimulated (J) conditions compared with wild-type GLUT4. Data were from nine cells (IR-basal), 12 cells (IR-insulin), 18 cells (F$^5$QQA-GLUT4 basal conditions) or 15 cells (F$^5$QQA-GLUT4, insulin stimulation) from three independent experiments. In E–H, every point represents one single cell. **P*<0.01, ***P*<0.0001; two-tailed paired Student's *t*-test. Data are mean±s.d.

protein molecules per cluster and the fraction of total molecules found in clusters were both decreased to 2.68±0.33 and 62±5%, respectively, after MβCD treatment (Fig. 4E). These data demonstrate that destruction of lipid rafts strongly influenced the nanoscale organization of F$^5$QQA-GLUT4 in cells under basal conditions, resulting in smaller and denser clusters of the GLUT4 mutant on the plasma membrane (Fig. 4F,G; Fig. S3C). Moreover, in the absence of lipid rafts, the proportion of the total number of molecules found in small clusters increased to 77.5%, and those in middle-sized (the average number of proteins per cluster ranged from 7 to 18) and large clusters (the average number of proteins per cluster ranged from 19 to 25) decreased to 21.4% and 1.1%, respectively (Fig. 4H).

## DISCUSSION

GLUT4, a high-affinity glucose transporter, has been extensively investigated as a crucial player in glucose metabolism and insulin resistance. Many studies have reported that GLUT4 translocates to and fuses with the plasma membrane, and that this process is controlled by insulin or disease states, such as insulin resistance. Because the plasma membrane provides a foundational platform for GLUT4 function, the distribution of GLUT4 on the plasma membrane could be altered by hormone stimulation or insulin resistance.

Thus, we used dSTORM to investigate the spatial organization of plasma-membrane-fused GLUT4 at the single-molecule level, with

Journal of Cell Science (2017) 130, 396-405 doi:10.1242/jcs.192450

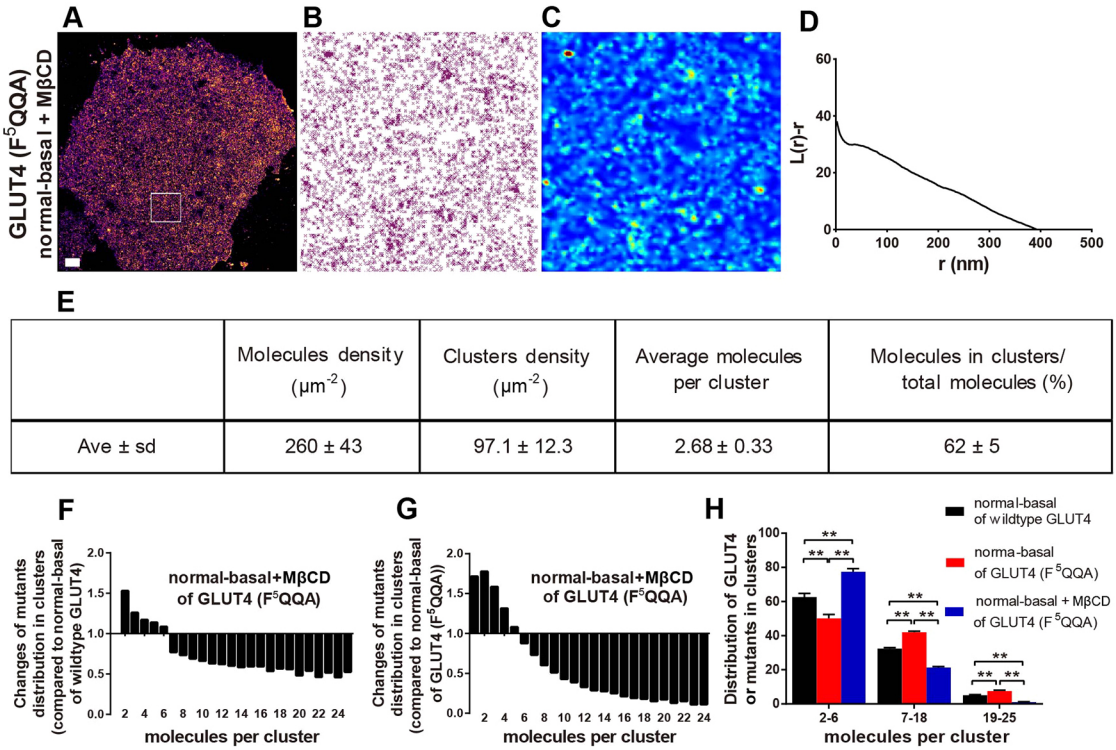


| | Molecules density ($\mu m^{-2}$) | Clusters density ($\mu m^{-2}$) | Average molecules per cluster | Molecules in clusters/ total molecules (%) |
|---|---|---|---|---|
| Ave ± sd | 260 ± 43 | 97.1 ± 12.3 | 2.68 ± 0.33 | 62 ± 5 |

**Fig. 4. Lipid raft destruction disperses F$^5$QQA-GLUT4 distribution under basal conditions.** (A) Representative dSTORM images of the GLUT4 mutant distribution on the plasma membrane of adipocytes that stably expressed HA–F$^5$QQA-GLUT4–GFP and had been treated with MβCD under basal conditions. (B) Enlarged and background-adjusted images illustrated the GLUT4 mutant distribution patterns on the plasma membrane of the white-boxed regions (4×4 μm) shown in A. (C) Heat maps of GLUT4 mutant clustering from the white-boxed regions shown in A. The colors indicate the degree of clustering from low (blue) to high (red). (D) Representative plot of Ripley's *K* function analysis of the clustering abilities of the GLUT4 mutant in the white-boxed regions of A. *L*(*r*)-*r* (*y*-axis) represents the clustering ability, and *r* (*x*-axis) represents the radial scales of clustering. (E) Molecule density, cluster density, mean molecules per cluster and the percentage of total molecules found in clusters of the GLUT4 mutant in adipocytes were determined from dSTORM images (A). Ave, average (mean). (F) Changes in the GLUT4 mutant in clusters under basal conditions shown in A compared with wild-type GLUT4 under basal conditions without MβCD treatment. (G) Changes in the GLUT4 mutant in clusters under basal conditions shown in A compared with the F$^5$QQA-GLUT4 mutant under basal conditions without MβCD treatment. (H) Quantification of the percentage of GLUT4 molecules in clusters having sizes between 2 and 6, 7 and 18, or 19 and 25 molecules relative to the total number of GLUT4 molecules under normal-basal conditions for wild-type GLUT4 or normal-basal and normal-basal+MβCD conditions for F$^5$QQA-GLUT4. Data were from 16 cells from three independent experiments. **P*<0.01, ***P*<0.0001; two-tailed paired Student's *t*-test.

a resolution of about 20 nm. Super-resolution images showed that GLUT4 did not distribute homogeneously on the plasma membrane but that it formed clusters or remained as single protein molecules both in normal adipocytes and insulin-resistant adipocytes, consistent with the findings of previous studies based on traditional technologies. The primary estimate of clustering using Ripley's *K*-function indicates that GLUT4 was less clustered after insulin stimulation. Moreover, insulin resistance and mutations in the F$^5$QQI motif caused increased clustering of plasma membrane GLUT4. When lipid rafts were disrupted in basal adipocytes that stably expressed F$^5$QQA-GLUT4, the clustering ability of plasma membrane F$^5$QQA-GLUT4 was notably decreased to the level of that in normal cells in the insulin-stimulated state.

Additionally, quantitative analyses of dSTORM data allowed for evaluation of several parameters in order to describe the differences in the clusters in different states and to confirm the results of Ripley's *K* function analysis. In normal adipocytes, insulin stimulation decreased the population of GLUT4 molecules found in clusters by 12%, indicating that more single molecules existed outside of clusters after stimulation. Furthermore, the distribution of GLUT4 in differently sized clusters also changed with insulin stimulation; about 10% of the clustered GLUT4 shifted from large clusters to small clusters, consistent with the results of Ripley's *K* function analysis. This could explain why the mean number of molecules per cluster did not change markedly, even though both the protein density and cluster density increased by about 2.5-fold.

In insulin-resistant adipocytes, owing to the reduced cell sensitivity to insulin, insulin stimulation resulted in small changes in molecule clustering, molecule density, cluster density and the populations of molecules in clusters compared with normal cells. However, the changes in molecule density and cluster density in the insulin-resistant state compared with those in normal cells were inconsistent, and the shift of GLUT4 from small clusters into large clusters both under basal and insulin-stimulated conditions resulted in an increased mean number of GLUT4 molecules per cluster; this increase induced a more clustered distribution of GLUT4 on the plasma membrane in the insulin-resistant state. Hence, in addition to altering the translocation of GLUT4 to the plasma membrane, insulin resistance affected the spatial distribution of GLUT4, promoting clustering on the plasma membrane.

When the F$^5$QQI motif was mutated, the proportions F$^5$QQA-GLUT4 that were clustered or dispersed on the plasma membrane were similar to those for wild-type GLUT4; however, the mutation resulted in a more clustered distribution, as also confirmed by Ripley's *K* function analysis. We consider that the compromised clathrin-mediated endocytosis caused by the F$^5$QQI mutation increased the number of GLUT4 molecules on the plasma membrane. If so, the simple accumulation would induce the observed changes in the molecule

Journal of Cell Science (2017) 130, 396-405 doi:10.1242/jcs.192450

density and the cluster density when compared with wide-type GLUT4; however, we found that the molecule density and the cluster density increased to different extents (1.6-fold and 1.35-fold). Furthermore, the majority of GLUT4 on the plasma membrane does not colocalize with clathrin, and clathrin is recruited to pre-existing GLUT4 clusters to mediate GLUT4 endocytosis (Lizunov et al., 2013; Stenkula et al., 2010), which indicates that the GLUT4 clustering is less likely to be due to clathrin regulation. Thus, the accumulation of GLUT4 might not be the direct cause of the more-clustered distribution. As the protein concentration is high, protein–protein interactions can induce the formation of microdomains or clusters (Douglass and Vale, 2005; Lin and Shaw, 2005). Hence, we speculate that the GLUT4 accumulation on the plasma membrane induced by the $F^5$QQI motif mutation increased the GLUT4 concentration and then induced GLUT4 self-assembly or an interaction of GLUT4 with other clustering-associated factors. However, the exact modulation mechanism involved in this cluster regulation is still unknown and an interest for future study.

Lipid rafts play an important role in the insulin signaling pathway and GLUT4 endocytosis (Al-Hasani et al., 2002; Chiang et al., 2001; Ros-Baro et al., 2001). Several studies have examined the association between GLUT4 clusters and lipid rafts. Some studies have suggested that GLUT4 transiently associates with lipid rafts (Chiang et al., 2001; Saltiel and Pessin, 2003) but that depletion of cholesterol does not disrupt GLUT4 clusters on the surface of adipocytes (Lizunov et al., 2013). Based on the published literature, we speculate that the MβCD treatment used in those studies was too gentle to disrupt the lipid rafts or that the destruction of lipid rafts affects the exocytosis and endocytosis of GLUT4, and that GLUT4 clusters associated with clathrin could persist after MβCD treatment. Furthermore, the data analysis used in those studies could also be a primary reason for the contrasting findings because the TIRFM that they used might not have been sensitive enough to detect small changes in cluster density. Thus, in our study, 3T3-L1 adipocytes that stably expressed $F^5$QQA-GLUT4 were treated with 10 mM MβCD (to disrupt lipid rafts) only in the basal state. Removal of the complicated effects of lipid rafts in the insulin-stimulated state, along with Ripley's *K* function and further quantitative analysis using the GDSC plugin in ImageJ, indicated that destruction of lipid rafts dispersed $F^5$QQA-GLUT4 on the plasma membrane, indicating the role of lipid rafts in GLUT4 cluster maintenance.

In summary, we used dSTORM to investigate the distribution of plasma membrane GLUT4 and the morphological properties of GLUT4 clusters in 3T3-L1 adipocytes, and also to reveal the effects of insulin and insulin resistance on GLUT4 spatial organization by performing Ripley's *K* function and quantitative cluster analysis. Our data revealed detailed information regarding GLUT4 distribution, including the densities of protein molecules and clusters, the mean number of molecules per cluster and the distribution of GLUT4 clusters containing different numbers of proteins. Our results suggest that insulin stimulation increased the number but decreased the size of GLUT4 clusters on the plasma membrane. However, the opposite effects were observed in the insulin-resistant state. In addition, we identified that mutation of the $F^5$QQI motif caused increased GLUT4 clustering on the plasma membrane and that lipid raft destruction in adipocytes that expressed $F^5$QQA-GLUT4 induced a more dispersed distribution of the mutant protein. Hence, the clustering of GLUT4 in the membrane is influenced by the intrinsic properties of GLUT4 itself and membrane subdomains. Thus, our findings provide important insights into GLUT4 clustering and the pathogenesis of insulin resistance. Further studies are needed to determine whether the spatial organization of plasma membrane GLUT4 that occurs under insulin resistance is also found in clinical cases.

## MATERIALS AND METHODS

### Antibodies and reagents

The HA.11 anti-HA epitope mouse mAb was purchased from Covance. Rabbit anti-Akt (#9272, detecting all isoforms; 1:1000), rabbit anti-phosphorylated-Akt (at Ser473, #9271; recognizes corresponding phosphorylations of Akt1, Akt2 and Akt3; 1:1000), rabbit anti-phosphorylated-Akt (at Thr308, #9275, recognizes corresponding phosphorylations of Akt1, Akt2 and Akt3; 1:1000) and rabbit anti-phosphorylated-AS160 (at Thr642; #4288, 1:1000) antibodies were purchased from Cell Signaling Technology. The rabbit anti-AS160 antibody (#07-741, 1:1000) was purchased from Millipore, and mouse anti-β-actin antibodies were purchased from Santa Cruz Biotechnology. Alexa-Fluor-647 and puromycin were purchased from Invitrogen. Dulbecco's modified Eagle's medium (DMEM) was purchased from Hyclone (Thermo Scientific). Penicillin–streptomycin, calf serum and fetal bovine serum (FBS) were purchased from Biological Industries (Israel). Insulin was purchased from Roche (Basel, Switzerland). Dexamethasone was purchased from Adamas (Basel, Switzerland). 3-Isobutyl-1-methylxanthine, rosiglitazone, β-mercaptoethanol, glucose, glucose oxidase and catalase were all purchased from Sigma.

### Cell culture, adipocyte differentiation and stable cell line construction

3T3-L1 fibroblasts (American Type Culture Collection) were cultured in high-glucose (4.5 g/l) DMEM supplemented with 10% calf serum and penicillin–streptomycin. 3T3-L1 fibroblasts were induced differentiate into mature adipocytes, as previously described (Zeigerer et al., 2002). The plasmids for stable cell line construction were prepared based on wild-type HA–GLUT4–GFP and the $F^5$QQI mutant, as described previously (Blot and McGraw, 2006, 2008; Lampson et al., 2001); sequences were inserted into pBABEpuro using *BamH*I and *EcoR*I sites. AmphoPack packaging cells were transfected with the plasmids, and culture medium from the packaging cells, harvested between 24 and 48 h post-transfection, was used to infect 3T3-L1 cells. 3T3-L1 cells that stably expressed wild-type HA–GLUT4–GFP or the $F^5$QQI mutant were selected in medium with 8 µg/ml puromycin. The surviving cells were cultured to induce differentiation as normal.

### Sample preparation

In all experiments, the HA-epitope tag, representing GLUT4 (or GLUT4 mutant) on the plasma membrane was immunofluorescently labeled by an Alexa-Fluor-647-conjugated HA1.1 antibody without permeabilization. HA.11 anti-HA-epitope mouse mAbs were labeled with Alexa-Fluor-647 at an appropriate concentration. The mixture containing 40 µl anti-HA mAbs (1 mg/ml) and 0.12 µl Alexa-Fluor-647 (10 mg/ml, dissolved in DMSO) was kept on a rocking platform at room temperature for 2–2.5 h in the dark. The product of the reaction was filtered through an equilibrated Nap-5 gel column (GE Healthcare) by running two column volumes of PBS, and the eluent was collected in tubes (three drops/tube). The labeling ratios of the collected samples were calculated based on the absorbance at 280 nm (antibody) and 650 nm (maximum absorbance of Alexa-Fluor-647). Samples with a labeling ratio of 0.5–1 Alexa-Fluor-647 molecules per antibody were pooled together and used for fluorescent staining.

Mature adipocytes that stably expressed wild-type HA–GLUT4–GFP or $F^5$QQA-GLUT4 were digested and dropped onto pre-cleaned glass coverslips. In all experiments, adipocytes that had been incubated in serum-free DMEM for at least 2 h at 37°C under 5% $CO_2$ were further incubated with or without 100 nM insulin for 8 min (basal or insulin-stimulated conditions). Cells were washed with ice-cold PBS and fixed in 3.7% formaldehyde for 8 min on ice. After incubation with 5% bovine serum albumin for 15 min, cells were stained using HA 1.1-antibody–Alexa-Fluor-647 in the dark for 30 min at 37°C without permeabilization. Finally, the sample was washed with PBS three times.

In order to remove insulin from the culture, after harvesting and stimulation with 100 nM insulin for 8 min, medium containing insulin was replaced with harvest medium, and cells were cultured for another 30 min. The cells were then fixed and stained as described before. For experiments with MβCD treatment, cells were harvested and treated with 10 mM MβCD for 15 min at 37°C before fixing and staining.

For dSTORM imaging, oxygen-scavenging PBS [containing 140 mM β-mercaptoethanol, 0.5 mg/ml glucose oxidase, 40 µg/ml catalase and 10% (m/v) glucose (Sigma)] was dropped onto the microscope slide, and the slides were sealed with coverslips.

### Imaging

dSTORM imaging was performed on a Nikon Ti-E microscope with a 100× oil-immersion a total internal reflection fluorescence objective (Nikon, Japan) with a numerical aperture of 1.49. All the dSTORM data were acquired under total internal reflection fluorescence illumination mode. During imaging, a 640-nm laser (100 mW) and an electron-multiplying charge-coupled device (EMCCD; Photometrics, Cascade II) were used. A total of 5000 raw images were acquired per cell with an exposure time of 40 ms for the reconstruction of super-resolution images. One single dSTORM image was acquired in less than 5 min. During this time, the *z*-drift was eliminated using a Nikon Perfect Focus System, and the *x*–*y* drift was reduced through the stabilization of the clips on the stage.

To measure single-molecule localization precision, an appropriate concentration of Alexa-Fluor-647-conjugated HA.11 (about 7 nM) was incubated on the slide or cell surface for 30 min and imaged (Fig. S2A,C). The clusters of localization from repetitive localization of several single HA 1.1–Alexa-Fluor-647 molecules were aligned to generate a histogram, and the histogram was fitted by a Gaussian function to yield full-width at half-maximum (FWHM) values of 31 nm on the slide and 27 nm on the cell surface, respectively (Fig. S2B,D). These data indicated a precision of approximately 30 nm for our imaging system with the HA 1.1–Alexa Fluor 647 probe.

### Data analysis

For overall evaluation of GLUT4 spatial clustering on the plasma membrane (Figs 1D, 2D, 3D, 4D), Ripley's *K* function was used to analyze the degree of spatial clustering of randomly selected 4×4-µm$^2$ regions (nine regions per individual cell) in reconstructed images (McEvoy et al., 2010; Owen et al., 2010; Ripley, 1979). Ripley's *K* function was calculated using MATLAB as Eqn 1.

$$K(r) = A\sum_{i=1}^{n}\sum_{j=1}^{n}\left(\frac{\delta_{ij}}{n^2}\right), (i \neq j), \quad (1)$$

where $\delta_{ij}$=1 if $\delta_{ij}$<$r$, otherwise 0; A is the area, $n$ is the number of localizations, $r$ is the spatial scale (radius) for the *K* function calculation and $\delta_{ij}$ is the distance between points i and j. This essentially counts the number of other points encircled by concentric rings centered on each point. The *K* function was linear-transformed into *H* function according to Eqn 2.

$$L(r) - r = \sqrt{((K(r))/\pi)} - r. \quad (2)$$

For a random distribution of localizations, $L(r)$–$r$=0, for clustered particles, this value is positive. Edge-effects were negated by weighting edge points and cropping the image edges after the calculation. Values of $L(r)$ generated for each point were used to produce a cluster map by interpolating a surface plot with $L(r)$ as the *z*-axis (color scale). Then the cluster map was then thresholded to generate a binary map.

To analyze the molecules in clusters relative to the total molecules (represents the percentage of the molecules that contributed to forming clusters versus the total molecules on the plasma membrane; Figs 1H, 2H, 3H and 4E), we used a derived algorithm based on Ripley's *K* function (Owen et al., 2012b; Williamson et al., 2011). The value of $L(r)$ for each molecule can be calculated at a spatial scale, which is the actual radius of the clusters. Here, the spatial scale was set as 75 nm according to the distance threshold between two different molecules in every image, which was calculated by using 'the blink estimator' subset and was similar to the reported size of GLUT4 clusters (diameter, 90–170 nm) analyzed by performing fluorescence photoactivation localization microscopy (FPALM) in previous literature (Lizunov et al., 2013). The $L(r)$ for each molecule is calculated as:

$$K_i(75) = A\sum_{j=1}^{n}\left(\frac{\delta_{ij}}{n^2}\right), \quad (3)$$

where $\delta_{ij}$=1 if $\delta_{ij}$<75, otherwise 0;

and

$$L(75) = \sqrt{((K(75))/\pi)}. \quad (4)$$

Then the molecules with $L$(75)-75>0 were defined as the molecules in clusters and extracted to calculate the percentage of the molecules in clusters of the total molecules.

Pair correlation photoactivated localization microscopy (PC-PALM), a function subset in the ImageJ plugin GDSC-SMLM, was used to calculate the features of GLUT4 clusters, including the 'molecule density' (represents the number of molecules per µm$^2$; Figs 1E, 2E, 3E, 4E), 'cluster density' (represents the number of clusters per µm$^2$; Figs 1F, 2F, 3F, 4E), 'mean number of molecules per cluster' (represents the averaged molecules per cluster from an entire cell; Figs 1G, 2G, 3G, 4E) and the detailed distribution of GLUT4 clusters containing different numbers of molecules (Figs 1I,J, 2I,J, 3I,J, 4F–H). PC-PALM is used to analyze the auto-correlation of a set of localizations using pair correlation analysis and has been confirmed that it is adaptable to quantitative spatial analysis of dSTORM images (Puchner et al., 2013; Sengupta et al., 2013, 2011; Veatch et al., 2012). The detailed approaches are described as follows.

#### Step 1

The size of each pixel (160 nm/pixel), total gain (0.3 ADU/photon), exposure time (40 ms) and peak width (0.828 pixel) were used as inputs for the sample fitting process by GDSC-SMLM. For each frame, the location of each fluorescent label was identified and least-squares fitted to a Gaussian intensity peak, whose width was scaled according to the precision. Then, the blink rate and distance threshold of the fluorescent label were calculated and set as parameters in the following protein cluster analysis.

#### Step 2

PC-PALM was used to analyze the auto-correlation of a set of localizations using pair correlation analysis and has been confirmed that it is adaptable to quantitative spatial analysis of dSTORM images (Puchner et al., 2013; Sengupta et al., 2013, 2011; Veatch et al., 2012). We used the PC-PALM molecules subset and ran PC-PALM mode to filter fitting results from raw images to a set of coordinates with time and photo signal information (blinking rate of fluorophores). Then the localizations were drawn onto a binary image for the subsequent analysis. It is known that the blinking of the same fluorophore results in a single protein in a dSTORM image appearing as a cluster of peaks. For this analysis by using the PC-PALM molecules subset, peaks appearing in consecutive frames and within a radius covering 99% probability density of the two-dimensional Gaussian function for localization uncertainty were considered to be a single localization. Thus, the problem of over-counting can be circumvented by using the PC-PALM molecules subset and the blink-corrected image was produced for further analysis of clusters.

#### Step 3

The obtained corrected binary image was then analyzed by using the PC-PALM analysis subset to produce a g(r) correlation cure, which can be used to estimate the protein molecules that are randomly organized or not. If the molecules were organized non-randomly, we used the PC-PALM clusters subset and ran the pair-wise algorithm to calculate the features of the clusters containing the total number of molecules and clusters, as well as the 'mean number of molecules per cluster' and a histogram of cluster size. During this approach, the radius was defined according to the distance threshold of every image, which was calculated by using the 'the blink estimator' subset. The values of all the images obtained from different conditions ranged from 45 nm to 75 nm, which is similar to the reported size of GLUT4 clusters on the plasma membrane (diameter, 90–170 nm) analyzed by using FPALM in previous literature (Lizunov et al., 2013).

#### Step 4

To analyze the distribution of GLUT4 clusters that contained different numbers of molecules, the proportions of proteins contributing to different classes of clusters were extracted from the calculation results and normalized to the corresponding proportion in the basal state. A ratio of greater than 1 indicated that the proportion of proteins in the given class of clusters was

much higher than that in the basal state; conversely, a ratio of less than 1 indicated that the proportion of proteins in the corresponding cluster was lower than that in the basal state.

The data for quantitative analysis were acquired under the same conditions, and the samples were prepared using the same methods. Thus, the results from quantitative analysis in studies with super-resolution microscopy are indicative but reliable in comparative experiments and reflect the real changes in protein organization. Statistical analysis was performed using two-tailed paired Student's *t*-test.

#### Acknowledgements
We thank Prof. Samuel Cushman (National Institutes of Health, Bethesda, MD) for providing the GLUT4 construct; Timothy E. McGraw and Min Zhang for valuable and helpful discussions; Feng Wang and Chunyuan Zhou for dSTORM-data-related analysis; and Mingjun Cai, Junguang Jiang and Yangyue Xu for support on the dSTORM equipment.

#### Competing interests
The authors declare no competing or financial interests.

#### Author contributions
Conceptualization: L.G., H.W. and W.X.; Methodology: L.G., J.C., J.G., H.W. and W.X.; Software: L.G., J.C. and J.G.; Validation: L.G. and W.X.; Formal analysis: L.G. and W.X.; Investigation L.G.; Resources: L.G., H.W. and W.X.; Data curation: L.G., J.C., J.G., H.W. and W.X.; Writing – original draft preparation: L.G., H.W. and W.X.; Writing – review and editing: L.G., H.W. and W.X.; Visualization: L.G. and W.X.; Supervision: H.W. and W.X.; Project administration: H.W. and W.X.; Funding acquisition: W.X..

#### Funding
This work was financially supported by the Chinese Academy of Sciences (292013312D11004 to W.X.); the National Natural Science Foundation of China (81270919 to W.X.); and Natural Science Foundation of Yunnan Province (39Y33H521261 to W.X.).

#### Supplementary information
Supplementary information available online at
http://jcs.biologists.org/lookup/doi/10.1242/jcs.192450.supplemental

#### References
**Al-Hasani, H., Kunamneni, R. K., Dawson, K., Hinck, C. S., Müller-Wieland, D. and Cushman, S. W.** (2002). Roles of the N-and C-termini of GLUT4 in endocytosis. *J. Cell Sci.* **115**, 131-140.

**Bai, L., Wang, Y., Fan, J., Chen, Y., Ji, W., Qu, A., Xu, P., James, D. E. and Xu, T.** (2007). Dissecting multiple steps of GLUT4 trafficking and identifying the sites of insulin action. *Cell Metab.* **5**, 47-57.

**Blot, V. and McGraw, T. E.** (2006). GLUT4 is internalized by a cholesterol-dependent nystatin-sensitive mechanism inhibited by insulin. *EMBO J.* **25**, 5648-5658.

**Blot, V. and McGraw, T. E.** (2008). Molecular mechanisms controlling GLUT4 intracellular retention. *Mol. Biol. Cell* **19**, 3477-3487.

**Brown, D. A. and London, E.** (2003). Functions of lipid rafts in biological membranes. *Annu. Rev. Cell Dev. Biol.* **14**, 111-136.

**Chiang, S.-H., Baumann, C. A., Kanzaki, M., Thurmond, D. C., Watson, R. T., Neudauer, C. L., Macara, I. G., Pessin, J. E. and Saltiel, A. R.** (2001). Insulin-stimulated GLUT4 translocation requires the CAP-dependent activation of TC10. *Nature* **410**, 944-948.

**Douglass, A. D. and Vale, R. D.** (2005). Single-molecule microscopy reveals plasma membrane microdomains created by protein-protein networks that exclude or trap signaling molecules in T cells. *Cell* **121**, 937-950.

**Fazakerley, D. J., Naghiloo, S., Chaudhuri, R., Koumanov, F., Burchfield, J. G., Thomas, K. C., Krycer, J. R., Prior, M. J., Parker, B. L. and Murrow, B. A.** (2015). Proteomic analysis of GLUT4 storage vesicles reveals tumor suppressor candidate 5 (TUSC5) as a novel regulator of insulin action in adipocytes. *J. Biol. Chem.* **290**, 23528-23542.

**Gao, J., Wang, Y., Cai, M., Pan, Y., Xu, H., Jiang, J., Ji, H. and Wang, H.** (2015). Mechanistic insights into EGFR membrane clustering revealed by super-resolution imaging. *Nanoscale* **7**, 2511-2519.

**Gonzalez, E. and McGraw, T. E.** (2006). Insulin signaling diverges into Akt-dependent and-independent signals to regulate the recruitment/docking and the fusion of GLUT4 vesicles to the plasma membrane. *Mol. Biol. Cell* **17**, 4484-4493.

**Gustavsson, J., Parpal, S. and Strålfors, P.** (1996). Insulin-stimulated glucose uptake involves the transition of glucose transporters to a caveolae-rich fraction within the plasma membrane: implications for type II diabetes. *Mol. Med.* **2**, 367.

**Heilemann, M., van de Linde, S., Schüttpelz, M., Kasper, R., Seefeldt, B., Mukherjee, A., Tinnefeld, P. and Sauer, M.** (2008). Subdiffraction-resolution fluorescence imaging with conventional fluorescent probes. *Angew. Chem. Int. Ed.* **47**, 6172-6176.

**Huang, S., Lifshitz, L. M., Jones, C., Bellve, K. D., Standley, C., Fonseca, S., Corvera, S., Fogarty, K. E. and Czech, M. P.** (2007). Insulin stimulates membrane fusion and GLUT4 accumulation in clathrin coats on adipocyte plasma membranes. *Mol. Cell. Biol.* **27**, 3456-3469.

**Jiang, L., Fan, J., Bai, L., Wang, Y., Chen, Y., Yang, L., Chen, L. and Xu, T.** (2008). Direct quantification of fusion rate reveals a distal role for AS160 in insulin-stimulated fusion of GLUT4 storage vesicles. *J. Biol. Chem.* **283**, 8508-8516.

**Koumanov, F., Jin, B., Yang, J. and Holman, G. D.** (2005). Insulin signaling meets vesicle traffic of GLUT4 at a plasma-membrane-activated fusion step. *Cell Metab.* **2**, 179-189.

**Lampson, M. A., Racz, A., Cushman, S. W. and McGraw, T. E.** (2000). Demonstration of insulin-responsive trafficking of GLUT4 and vpTR in fibroblasts. *J. Cell Sci.* **113**, 4065-4076.

**Lampson, M. A., Schmoranzer, J., Zeigerer, A., Simon, S. M. and McGraw, T. E.** (2001). Insulin-regulated release from the endosomal recycling compartment is regulated by budding of specialized vesicles. *Mol. Biol. Cell* **12**, 3489-3501.

**Lin, J. and Shaw, A. S.** (2005). Getting downstream without a Raft. *Cell* **121**, 815-816.

**Lingwood, D. and Simons, K.** (2010). Lipid rafts as a membrane-organizing principle. *Science* **327**, 46-50.

**Lizunov, V. A., Matsumoto, H., Zimmerberg, J., Cushman, S. W. and Frolov, V. A.** (2005). Insulin stimulates the halting, tethering, and fusion of mobile GLUT4 vesicles in rat adipose cells. *J. Cell Biol.* **169**, 481-489.

**Lizunov, V. A., Stenkula, K., Troy, A., Cushman, S. W. and Zimmerberg, J.** (2013). Insulin regulates Glut4 confinement in plasma membrane clusters in adipose cells. *PLoS ONE* **8**, e57559.

**Martin, S., Millar, C. A., Lyttle, C. T., Meerloo, T., Marsh, B. J., Gould, G. W. and James, D. E.** (2000). Effects of insulin on intracellular GLUT4 vesicles in adipocytes: evidence for a secretory mode of regulation. *J. Cell Sci.* **113**, 3427-3438.

**McEvoy, A. L., Greenfield, D., Bates, M. and Liphardt, J.** (2010). Q&A: Single-molecule localization microscopy for biological imaging. *BMC Biol.* **8**, 106.

**Owen, D. J., Collins, B. M. and Evans, P. R.** (2004). Adaptors for clathrin coats: structure and function. *Annu. Rev. Cell Dev. Biol.* **20**, 153-191.

**Owen, D. M., Rentero, C., Rossy, J., Magenau, A., Williamson, D., Rodriguez, M. and Gaus, K.** (2010). PALM imaging and cluster analysis of protein heterogeneity at the cell surface. *J. Biophotonics* **3**, 446-454.

**Owen, D. M., Magenau, A., Williamson, D. and Gaus, K.** (2012a). The lipid raft hypothesis revisited–new insights on raft composition and function from super-resolution fluorescence microscopy. *Bioessays* **34**, 739-747.

**Owen, D. M., Williamson, D., Magenau, A., Rossy, J. and Gaus, K.** (2012b). Chapter eleven–optical techniques for imaging membrane domains in live cells (live-cell palm of protein clustering). *Methods Enzymol.* **504**, 221-235.

**Parton, R. G., Molero, J. C., Floetenmeyer, M., Green, K. M. and James, D. E.** (2002). Characterization of a distinct plasma membrane macrodomain in differentiated adipocytes. *J. Biol. Chem.* **277**, 46769-46778.

**Pontier, S. M., Percherancier, Y., Galandrin, S., Breit, A., Galés, C. and Bouvier, M.** (2008). Cholesterol-dependent Separation of the β2. *J. Biol. Chem.* **283**, 24659-24672.

**Puchner, E. M., Walter, J. M., Kasper, R., Huang, B. and Lim, W. A.** (2013). Counting molecules in single organelles with superresolution microscopy allows tracking of the endosome maturation trajectory. *Proc. Natl. Acad. Sci. USA* **110**, 16015-16020.

**Ripley, B.** (1979). Tests of 'Randomness' for spatial point patterns. *J. R. Stat. Soc. Ser. B (Methodological)*, **41**, 368-374.

**Ros-Baro, A., Lopez-Iglesias, C., Peiro, S., Bellido, D., Palacin, M., Zorzano, A. and Camps, M.** (2001). Lipid rafts are required for GLUT4 internalization in adipose cells. *Proc. Natl. Acad. Sci. U. S. A.* **98**, 12050-12055.

**Saltiel, A. R. and Pessin, J. E.** (2003). Insulin signaling in microdomains of the plasma membrane. *Traffic* **4**, 711-716.

**Sengupta, P., Jovanovic-Talisman, T., Skoko, D., Renz, M., Veatch, S. L. and Lippincott-Schwartz, J.** (2011). Probing protein heterogeneity in the plasma membrane using PALM and pair correlation analysis. *Nat. Methods* **8**, 969-975.

**Sengupta, P., Jovanovic-Talisman, T. and Lippincott-Schwartz, J.** (2013). Quantifying spatial organization in point-localization superresolution images using pair correlation analysis. *Nat. Protoc.* **8**, 345-354.

**Slot, J. W., Geuze, H. J., Gigengack, S., Lienhard, G. E. and James, D. E.** (1991). Immuno-localization of the insulin regulatable glucose transporter in brown adipose tissue of the rat. *J. Cell Biol.* **113**, 123-135.

**Stenkula, K. G., Lizunov, V. A., Cushman, S. W. and Zimmerberg, J.** (2010). Insulin controls the spatial distribution of GLUT4 on the cell surface through regulation of its postfusion dispersal. *Cell Metab.* **12**, 250-259.

**Veatch, S. L., Machta, B. B., Shelby, S. A., Chiang, E. N., Holowka, D. A. and Baird, B. A.** (2012). Correlation functions quantify super-resolution images and estimate apparent clustering due to over-counting. *PLoS ONE* **7**, e31457.

**Watson, R. T., Shigematsu, S., Chiang, S.-H., Mora, S., Kanzaki, M., Macara, I. G., Saltiel, A. R. and Pessin, J. E.** (2001). Lipid raft microdomain compartmentalization of TC10 is required for insulin signaling and GLUT4 translocation. *J. Cell Biol.* **154**, 829-840.

**Williamson, D. J., Owen, D. M., Rossy, J., Magenau, A., Wehrmann, M., Gooding, J. J. and Gaus, K.** (2011). Pre-existing clusters of the adaptor Lat do not participate in early T cell signaling events. *Nat. Immunol.* **12**, 655-662.

**Xiong, W. Y., Jordens, I., Gonzalez, E. and McGraw, T. E.** (2010). GLUT4 is sorted to vesicles whose accumulation beneath and insertion into the plasma membrane are differentially regulated by insulin and selectively affected by insulin resistance. *Mol. Biol. Cell* **21**, 1375-1386.

**Zeigerer, A., Lampson, M. A., Karylowski, O., Sabatini, D. D., Adesnik, M., Ren, M. and McGraw, T. E.** (2002). GLUT4 retention in adipocytes requires two intracellular insulin-regulated transport steps. *Mol. Biol. Cell* **13**, 2421-2435.

**Supporting Information**

# Super-resolution microscopy reveals the reorganization of GLUT4 on plasma membrane regulated by insulin resistance

Lan Gao[1,2], Junling Chen[2,3], Jing Gao[2,3], Hongda Wang[3],* & Wenyong Xiong[1],*

[1] State Key Laboratory of Phytochemistry and Plant Resources in West China, Kunming Institute of Botany, Chinese Academy of Sciences, Kunming, YN 650201, P.R. China

[2] Graduate University of Chinese Academy of Sciences, Beijing 100049, P.R. China

[3] State Key Laboratory of Electroanalytical Chemistry, Changchun Institute of Applied Chemistry, Chinese Academy of Sciences, Changchun, JL 130022, P.R. China

*** Author for correspondence:**

Prof. Wenyong Xiong, Ph.D.

Kunming Institute of Botany, Chinese Academy of Sciences

132 Lanhei Road, Kunming, Yunnan 650201, China

Tel: 0086-871-65216939， Fax: 0086-871-65216750

Email: xiong.wenyong@mail.kib.ac.cn

Or

Prof. Hongda Wang, Ph.D.

Changchun Institute of Applied Chemistry, Chinese Academy of Sciences

5625 Renmin Rd., Changchun, Jilin 130022, China

Tel: 0086-0431-85262684， Fax: 0086-85262864

Email: hdwang@ciac.ac.cn

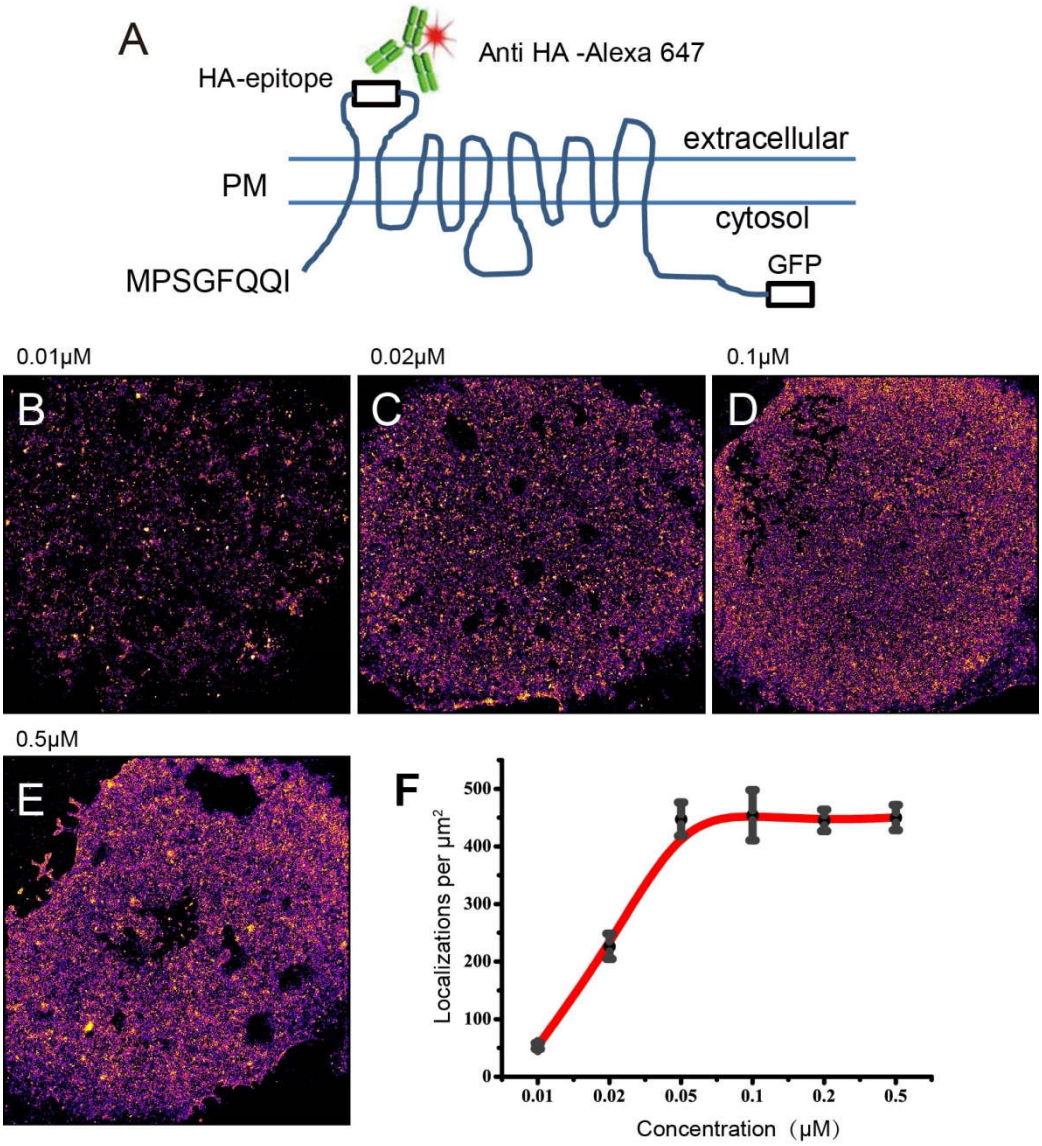


Figure S1. A. Structural diagram of the HA-GLUT4-GFP protein. The $F^5QQI$ motif is indicated, and the positions of the HA-epitope tag and GFP are shown. B-E. dSTORM images GLUT4 on the PM of insulin-stimulated adipocytes treated with different concentrations of anti-HA 1.1-Alexa Fluor 647 (0.01- 0.5 μM). F. Localization density of GLUT4 on the PM of insulin-stimulated adipocytes treated with different concentrations of anti-HA 1.1-Alexa Fluor 647 (0.01- 0.5 μM); at an anti-HA 1.1-Alexa Fluor 647 concentration of about 0.05 μM, the number of localizations per unit of cell membrane area, as determined by dSTORM, was saturated.

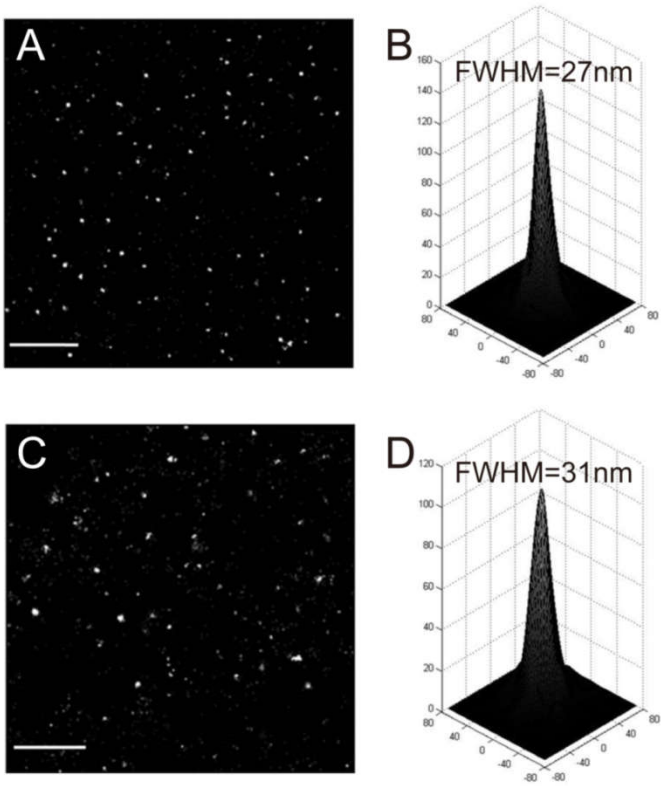


Figure S2. Measurement of the localization precision of a single Alexa Fluor 647-conjugated anti-HA.11 monoclonal antibody (mAb) molecule on a coverslip or the cell surface. (A) Typical dSTORM image of Alexa Fluor 647-conjugated anti-HA.11 mAbs at an appropriate concentration (~7 nM) on a clean coverslip. Each spot in the image represents a cluster of localizations from a single Alexa Fluor 647-conjugated antibody molecule. (B) Two-dimensional histograms of the localizations were generated by aligning 50 single antibody molecules, and the localization precision of 27 nm was determined by measuring the full-width at half-maximum (FWHM). (C，D) The localization precision of a single Alexa Fluor 647-conjugated anti-HA.11 mAb molecule on the 3T3-L1 adipocyte membrane. The FWHM was 31 nm. Scale bar: 2 μm.

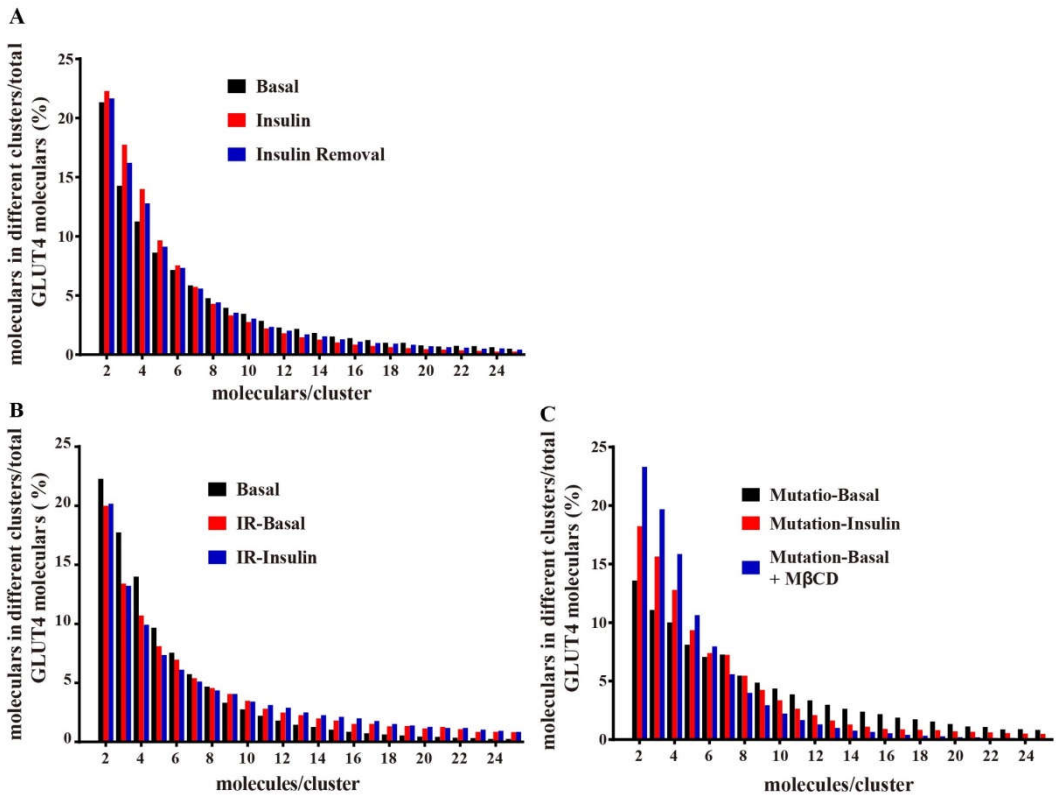


Figure S3. The entire GLUT4 molecules distribution of different sizes of clusters in all conditions studied: (A) wide-type GLUT4 on the PM of normal cells; (B) wide-type GLUT4 on the PM of insulin-resistant cells; (C) $F^5$QQI-GLUT4 on the PM of normal cells.

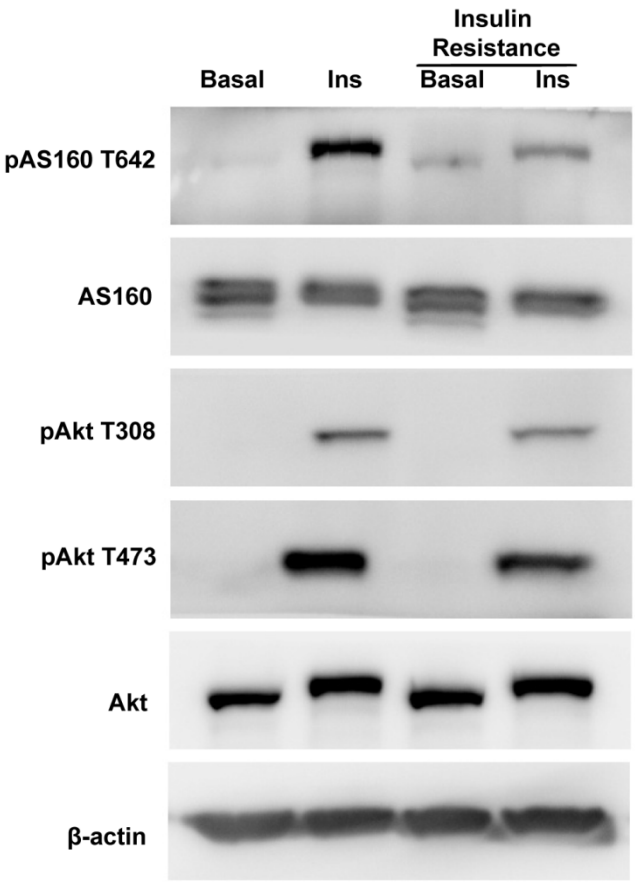


Figure S4. Representative western blot of screened proteins involved in the insulin signaling pathway in insulin-resistant adipocytes. Insulin signaling was monitored by measuring phosphorylation of Akt at Thr-308 and Ser-473 and AS160 at Thr-642 in response to 100 nM insulin. Total levels of Akt and AS160 were assessed in all conditions, and β-actin was used as a control.

Table S1. Compare of corresponding data in Figure 1 and Figure 3.

| | Widetype GLUT4 | | GLUT4 ($F^5QQA$) | |
|---|---|---|---|---|
| | Normal-Basal | Normal-Insulin | Normal-Basal | Normal-Insulin |
| Molecules Density | 90 ± 41 | 229 ± 48 | 184 ± 37 | 363 ± 123 |
| Clusters Density | 31.4 ± 13.2 | 79.6 ± 12.7 | 49.8 ± 11.0 | 108.9 ± 33.4 |
| Average molecules per cluster | 2.79 ± 0.39 | 2.87 ± 0.36 | 3.73 ± 0.36 | 3.44 ± 0.33 |
| Molecules in clusters/total molecules | 78% ± 5% | 66% ± 2% | 80% ± 4% | 63% ± 5% |